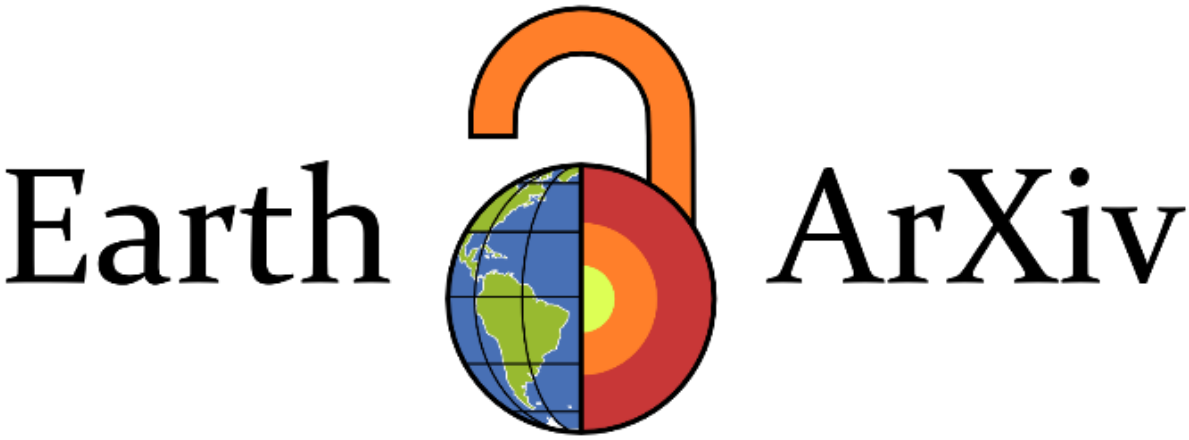

Half of anthropogenic warming now caused by fossil fuels

Nathaniel Tarshish[1*], David M. Romps[23] and Inez Fung[2]

[1]Department of Earth and Planetary Sciences, Harvard University, Cambridge, MA, USA.
[2]Department of Earth and Planetary Science, University of California, Berkeley, CA, USA.
[3]Climate and Ecosystem Sciences Division, Lawrence Berkeley National Laboratory, Berkeley, CA, USA.

*Corresponding author(s). E-mail(s): ntarshish@g.harvard.edu;
Contributing authors: romps@berkeley.edu; ifung@berkeley.edu;

Abstract

Using recent emissions data and a climate emulator, the 2020s are identified as the decade during which fossil-fuel combustion likely becomes the dominant driver of global warming. Prior to 2020, other activities – including agricultural, forestry, and other land use – were likely the major contributors to warming. Before 1980, the net effect of fossil fuels was likely cooling, as their generation of sulfate aerosols dominated over the cumulative effect of their greenhouse gases. In recent decades, the accumulation of long-lived carbon dioxide in the atmosphere, alongside a decrease in sulfate emissions, has resulted in a substantial increase in the warming attributable to fossil fuels. This has led to fossil fuels and other activities contributing about equally to anthropogenic warming at present. On the other hand, fossil fuels are responsible for the vast majority of committed warming.

Keywords: temperature, warming, fossil fuels, agriculture, land use

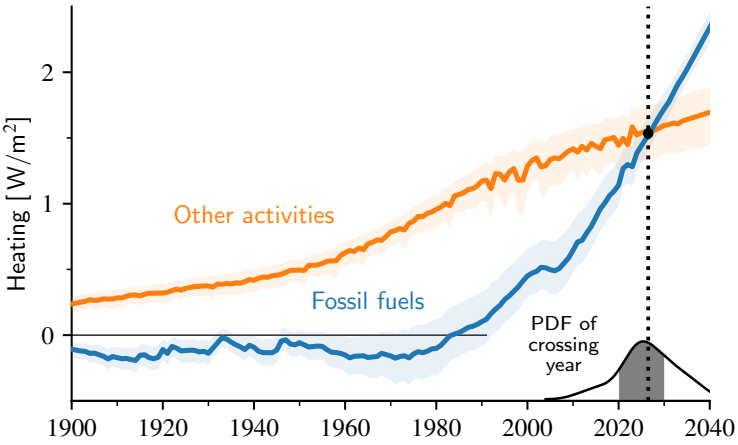

Fig. 1: Heating (i.e., effective radiative forcing) attributed to burning fossil fuels (blue) versus all other activities (orange) over the historical period. Solid lines are the medians of the climate model ensemble and shading indicates interquartile ranges. The probability distribution function (PDF) of the year in which fossil fuels become the primary source of warming is also shown with the median indicated by a dashed line.

It is commonly asserted that fossil fuels are the primary cause of anthropogenic warming, e.g., as stated by the U.S. National Climate Assessment [1], EPA [2], NASA [3], and United Nations [4]. Fossil fuel is indeed the main source of carbon dioxide and a major source of methane and nitrous oxide [5]. However, fossil fuel is also the dominant source of sulfate aerosols, tiny particles that *cool* by reflecting sunlight, directly and by increasing the number of water droplets in clouds [6].

The net anthropogenic effective radiative forcing (ERF, also referred to here as the "heating") for 2023 (relative to 1750) is estimated to be 2.79 [90% CI: 1.78 to 3.61] W m^{-2}, which includes a substantial cooling from anthropogenic aerosols [7–10] estimated to be −1.18 [90% CI: −2.10 to −0.49] W m^{-2} [11]. A considerable portion of the gross heating derives from non-fossil-fuel activities, particularly agriculture and land use, while nearly all the aerosol cooling is due to fossil fuels. The fossil-fuel origin of this cooling has raised questions about the extent to which historical temperature increases have been driven by fossil fuels [12, 13], especially given that fossil-fuel CO_2 emissions were lower, and sulfate emissions higher, in the past.

Notably, the Intergovernmental Panel on Climate Change (IPCC) has not assessed whether fossil-fuel combustion is the dominant source of present-day global warming. Instead, the IPCC Sixth Assessment (AR6) report follows the standard practice of attributing heating to the concentrations of individual greenhouse gases and aerosols [5]. Since current concentrations are due to both fossil fuels and other activities, the impact of fossil fuels alone is unclear. This present study fills this gap by providing a probabilistic evaluation, consistent with the state of the science in AR6, of the contribution of fossil fuels to global warming over the industrial era.

Fossil fuels shift from cooling to warming

The impact of fossil fuel emissions on global warming is analyzed here using a simple climate model ensemble [14]. Recent IPCC reports prominently feature this same model, the Finite-amplitude Impulse Response (FaIR) emulator [15–17], which was specifically developed to assess global-mean climate variations caused by greenhouse gases and aerosols [18–20]. Experiments are performed here with an 841-member ensemble [14], calibrated to reproduce historical observations and AR6-assessed ranges for key climate metrics, including the uncertainty of the magnitude of aerosol cooling (see Materials and Methods).

Historical emissions data are sourced from the same datasets used in AR6 [21, 22], updated to the present day as per the 2023 Indicators of Global Climate Change (IGCC) report [11, 23–26]. Future emissions and gaps in historical data, arising from reporting delays, are estimated by linear extrapolation of the past decade's emissions for each species and activity. When all emission sources are considered, the FaIR ensemble agrees with the IGCC on the central estimates and uncertainties for total and per-species radiative forcings (refer to Supplementary Figure 7).

Anthropogenic heating is attributed here to the burning of fossil fuels and other activities using two experiments with FaIR: one driven solely by historical fossil-fuel emissions, and another driven by historical emissions from all other activities. Those other activities are agriculture, forestry, other land uses (AFOLU), cement calcination, biomass combustion, certain mineral and chemical processes, waste handling, landfills, and emissions

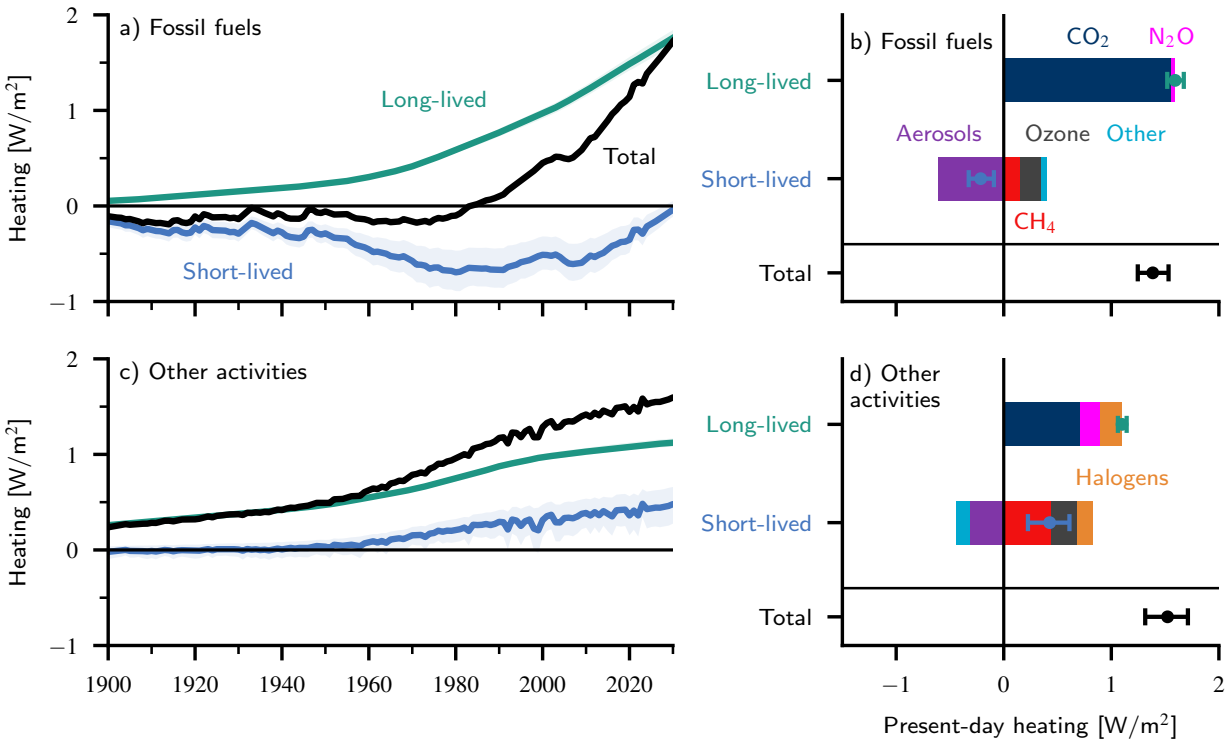

Fig. 2: a) Heating from long-lived fossil-fuel greenhouse gases (green) has accumulated over time, overcoming cooling due to co-emitted short-lived species (blue) around 1980. b) The long-lived component of fossil fuels is predominantly from CO_2, while aerosols have dominated the short-lived species. c) Warming from other activities (primarily agriculture and land use) has grown relatively slowly since 1980 and has never been substantially masked by short-lived cooling. d) The short- and long-lived heating due to other activities are both positive and involve a variety of species. Shadings and whiskers indicate interquartile ranges.

of halogenated gases. For a detailed breakdown of the emissions sources and classification, refer to Materials and Methods. The FaIR ensemble solves for the gas concentrations, forcings, and global temperature anomaly given each experiment's subset of historical emissions.

Due to nonlinear effects (primarily from atmospheric chemistry), the sum of the radiative heating from these two separate experiments exceeds the heating due to all emissions by 12% in 2023 (see Supplementary Figure 11 and Table 2). Since this nonlinear component of the total heating is generated if and only if both sets of emissions are present, it is attributed here in equal parts to fossil fuels and other activities. The heating timeseries for the two separate experiments are reduced by equal (yet time-varying) amounts so that their sum matches the heating timeseries resulting from when FaIR is driven by all emissions combined (see Methods).

Figure 1 shows the resultant heating timeseries for the fossil-fuel experiment in blue and for other activities in orange. The median estimate of net fossil-fuel radiative forcing is negative, averaging -0.1 W m^{-2}, up until the early 1980s. This suggests that fossil fuels contributed to a global cooling effect during much of the 20th century, partially offsetting warming from other sources. From the 1980s onward, heating from fossil fuels has increased sharply, rising at 0.3 W m^{-2} per decade, and culminating in a total of 1.4 W m^{-2} by 2024. In contrast, the heating from other sources (mainly AFOLU) has been consistently positive throughout the 20th century, with a slower average increase of 0.1 W m^{-2} per decade since 1980.

To understand changes in warming over time, Figure 2 categorizes radiative forcings as either long-lived or short-lived. All species, except for CO_2, N_2O, and halogenated gases that have lifetimes of a century or more are considered short-lived. Short-lived gas concentrations are proportional to recent emissions levels, while long-lived gas concentrations are determined by cumulative emissions over the entire industrial period.

At the turn of the 20th century, annual CO_2 emissions from fossil fuels and other activities were the same order of magnitude (Supplemental Figure 4). However, the heating effect from fossil-fuel CO_2 was minimal because not enough time had passed since the start of industrialization for those emissions to accumulate

significantly. In contrast, CO_2 from non-fossil sources had been accumulating from deforestation over the prior centuries, resulting in substantial radiative forcing by 1900.

Sulfate concentrations, however, depend only on recent emissions, meaning that aerosol cooling from fossil fuels had a substantial influence even at the onset of industrialization. Additionally, the fuel mix in the early 20th century had a higher sulfur content than present-day [22], further enhancing the relative importance of aerosol cooling. As a result, fossil fuels yielded a net cooling over much of the 20th century: short-lived cooling outweighed the gradual build up of long-lived greenhouse gases, primarily CO_2. This dynamic shifted around 1980 when the fossil-fuel CO_2 had finally accumulated to sufficient levels to overcome aerosol cooling and produce net heating.

The sharp increase in fossil-fuel-related heating since then can be attributed to a significant rise in long-lived greenhouse gas emissions, and also a reduction in short-lived cooling effects, primarily from a decrease in sulfate aerosols (Supplemental Figure 9). Stricter emissions standards that led to the adoption of flue-gas desulfurization at coal-fired power plants and limits on fuel sulfur content are responsible for this aerosol decline [27].

Currently, the net effect of short-lived forcings from fossil fuels is negligible, as the cooling from aerosols is largely balanced by heating from ozone and methane (Figure 2b). Therefore, existing fossil-fuel infrastructure is adding additional heating that can be thought of, to good approximation, as entirely long-lived and due to CO_2. In contrast, much of the heating due to other activities activities is short-lived. In further contrast to fossil fuels, the growth in the long-lived component of heating from other activities has been relatively modest over recent decades.

The closest comparison to our findings is work of ref. [13], which approximated fossil fuel's share of each species' current radiative forcing by the fraction of fossil fuel's cumulative emissions of that species since the preindustrial. That method does not account for the natural sinks of those species, the timescales of those sinks, or the time series of emissions, all of which are accounted for here. Whereas the approximate method estimated that only 34% of anthropogenic heating in 2019 was due to fossil fuels [13], the median fraction for 2019 is found here to be 42%, approaching the parity of 50% that is most likely to occur in the current decade.

Fossil fuels now at parity with other activities

Figure 1 illustrates that the 2020s are the most likely decade for fossil fuels to overtake other activities to become the leading cause of global warming. The probability distribution function (PDF) of crossing times (from the 841 members of the ensemble) peaks this decade with a mode of 2024 and median of 2026. In addition, the ensemble gives a 52% chance that the crossing occurs this decade.

The range of predicted crossing times in the ensemble reflects uncertainties within the climate system, primarily related to the direct and indirect radiative effects of aerosols (see Supplemental Figure 6 and Table 2). Figure 1, however, does not account for uncertainties in the emissions data. Emissions uncertainties are expected to be symmetrical [11, 25], such that accounting for them would broaden the PDF of crossing times but not shift the peak, meaning that the 2020s would still be the most likely decade for fossil fuels to begin dominating warming.

Finally, we note that reporting practices make it unclear whether certain industrial process and product use (IPPU) emissions originate from fossil fuels [28]. In Figure 1, these ambiguous IPPU emissions are categorized as non-fossil. If these ambiguous IPPU emissions are reclassified as originating from fossil fuels, the median crossing year moves to 2025 (refer to Supplemental Figure 12). In either case, this decade is the most likely time for the transition to fossil-fuel dominance.

Committed warming dominated by fossil fuels

While fossil fuels are just now rivaling other activities in terms of instantaneous heating, fossil fuels began dominating the heating from long-lived species in the early 2000s. This means that the commitment to future temperatures was already dominated by fossil fuels around the turn of the century. Today, in 2024, the long-lived heating from fossil fuels is roughly 50% larger than that of other activities.

The previous sections separated species into short-lived and long-lived using a timescale of a century, but it is possible to consider the commitment to temperature anomalies at much longer timescales. In the centuries beyond 2100, "long-lived" species like N_2O and many types of halogens are effectively removed from the atmosphere, leaving CO_2 responsible for the vast majority of the heating. The cumulative emissions of CO_2 due to fossil fuels surpassed other activities in the late 1980s, so the multi-century heating commitment has been dominated by fossil fuels for several decades.

Furthermore, the CO_2 emissions from fossil fuels are fundamentally different from the CO_2 emissions from other activities, which come mainly from AFOLU. If future food production shifts away from land-intensive

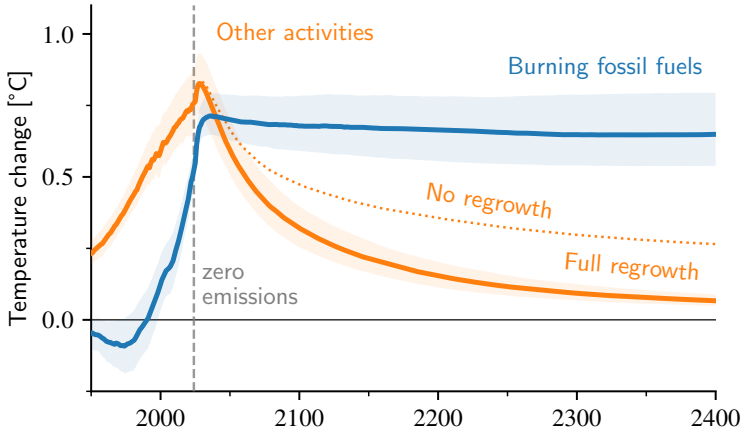

Fig. 3: The temperature response to presently ceasing emissions in scenarios driven solely by burning fossil fuels (blue) and all other activities (orange), respectively. In the latter case, the fate of agriculture and land-use CO_2 emissions is illustrated by scenarios with no (dashed) and full (solid) regrowth from ecosystem restoration.

practices, past land-use CO_2 emissions would largely be removed from the atmosphere due to regrowth on a centennial timescale [29]. On the other hand, carbon dioxide from fossil fuels is primarily taken up by the ocean, on a set of timescales ranging from centuries to many millennia [30].

Figure 3 explores the temperature commitments from fossil fuels and other activities. In these experiments, emissions are ceased in 2024. Although the present-day total radiative forcings in each experiment are similar (as shown in Figure 1), the temperature increase in the fossil-fuel case lags by 0.2 K due to the ocean's thermal inertia.

The temperature anomaly due to fossil fuels remains essentially constant over the coming centuries. Radiative forcing, on the other hand, is roughly halved in this scenario over the following centuries due to CO_2 uptake by natural carbon sinks (Supplementary Figure 10). However, this decline in heating is balanced by a weakening of the deep-ocean heat sink, which is substantially moderating surface temperatures at present. The compensation between the declining source and sink of heat results in a time-invariant temperature commitment from burning fossil fuels [31, 32].

In contrast, the temperature change due to other activities declines steeply after emissions cessation, particularly under the assumptions of strong regrowth (see Methods). Large declines in radiative forcing due to the shorter-lived nature of these forcings dominate over the waning oceanic heat sink, leading to a global-average temperature that approaches pre-industrial levels on this multi-century timescale. Thus, the commitment to temperature anomalies on multi-centennial timescales [33] is overwhelmingly due to fossil fuels.

Discussion

These findings underscore the urgency of reducing the burning of fossil fuels relative to other mitigation activities. Fossil-fuel heating has grown rapidly over the last few decades, yielding a temperature increase that is effectively permanent on civilizational timescales absent negative-emissions technologies. At the same time, the analysis here challenges the prevailing belief that fossil-fuel combustion was the main driver of 20th-century warming [1–4]. Until this decade, it is likely that fossil fuels were *not* the primary cause of global warming. Looking forward, however, as the reliance on fossil fuels continues [34] and tighter emissions controls on sulfate aerosols are implemented [35], the heating from fossil fuels will increasingly dominate future warming.

Materials and Methods

Historical emissions

Emissions of greenhouse gases and aerosols from 1750 to the present are compiled using the methodology described in ref. [14], which relies on the same datasets employed in AR6, updated to reflect current emissions as reported in the latest IGCC report [11]. In addition to replicating the total emissions reported in ref. [14], we use supplemental data to distinguish between emissions from fossil fuels and those from non-fossil-fuel sources.

Fossil-fuel emissions include all sources except those from agriculture, forestry, and other land uses (AFOLU); cement calcination and other material processes; specific industrial chemical and mineral processes; biomass fires and waste-to-energy; waste management; landfills; and halogenated gases. Guided by the IPCC's common reporting framework [28], the fossil-fuel category defined here covers all energy sector emissions except for biomass combustion and includes a subset of the emissions due to industrial processes (Sector 2), waste (Sector 6), and other activities (Sector 7).

All CO_2 emissions data are taken from the 2023 Global Carbon Project (GCB) [36]. Fossil-fuel CO_2 emissions are taken from the fossil-only category of the GCB dataset, while non-fossil-fuel CO_2 emissions are sourced from GCB's land-use-change and calcination datasets.

The Community Emissions Database (CEDS) [22, 26] is used to source emissions from 1750 to 2019 of black carbon (BC), organic carbon (OC), NH_3, NO_x, SO_2, and volatile organic compounds (VOC). From 2019 to 2022, the CEDS data are projected forward using emission factors based on mobility data from the two-year blip scenario of COVIDMIP [37] following the methodology of ref. [14]. CEDS covers all activities except for biomass fires. The CEDS dataset categorizes fossil-fuel emissions by sector, detailed in Table 1. Biomass combustion emissions are excluded from the energy sector using data from the alternative "by fuel" CEDS dataset. The role of fossil fuels in emissions from certain industrial sectors remains ambiguous due to the diverse chemical processes aggregated within these sectors. While some of these processes undoubtedly use fossil fuels as feedstocks, precise attribution is not available in the CEDS dataset. In the primary results and figures, these ambiguous sectors are grouped with non-fossil activities. However, attributing these ambiguous emissions to fossil fuels instead does not affect the conclusions (see Supplemental Figure 12).

The primary source for CH_4 and N_2O emissions is PRIMAP-Hist (i.e., the "third-party" version) [23, 38], supplemented by CEDS data where necessary. PRIMAP data are grouped at the IPCC sectoral level, necessitating a further breakdown for the waste and industrial sector emissions, which include fossil, biogenic, and ambiguous sources. CEDS, which provides data at the finer subsector level, is used to estimate the fractional contribution of the above sources to the PRIMAP sector totals. The CEDS record, however, only goes back to 1970. To disaggregate the PRIMAP waste emissions before 1970, the fraction of PRIMAP sectoral emissions due to waste combustion is assumed to be constant prior to 1970. A similar approach is used to categorize non-fossil and ambiguous activities within the Industrial Process and Product Use (IPPU) sector based on CEDS subsector data, with these respective emissions fractions assumed constant before 1970.

Emissions from biomass burning of all species other than CO_2 (i.e., BC, CH_4, CO, NH_3, NO_x, OC, and SO_2) are sourced from the Global Fire Emissions Dataset [24] and from BB4CMIP [21]. Halogenated gas emissions (F-gases) come from ref. [14] and are inverted from observed concentrations using IPCC assessed lifetimes, except for SF_6 and NF_3, which are available in the PRIMAP-Hist dataset. Future emissions and historical data gaps due to reporting delays are addressed by linear extrapolation based on per-species decadal emissions trends.

Climate emulator

Reduced-complexity models are well-suited to attributing radiative forcing to specific activities because they can be used in large ensembles that span key uncertainties and can be calibrated against observed data and other climate metrics [14, 19]. Specifically, the AR6 WG1 report included a detailed calibration of several such models, including the Finite-amplitude Impulse Response (FaIR) model, used in this study [39]. Simulations are performed here with the latest version (2.1.0) [20], which has been calibrated to observations updated through 2022 in ref. [14] to provide an 841-member AR6-consistent ensemble (v1.4.1). The complete calibration process is documented in [14] and summarized here for clarity.

FaIRv2.1 simulates global-average quantities with a three-box ocean model and a basic carbon-cycle parameterization with four uptake timescales [18, 20, 40]. Those four atmospheric lifetimes of CO_2 vary based on atmospheric levels, global-mean temperature, and the cumulative uptake by land and oceans. Methane's lifetime depends on the global-mean temperature and the presence of other chemically-active species, including methane itself, as illustrated in Supplementary Figure 8. Aside from CO_2 and CH_4, all other greenhouse gases (GHGs) decay at a constant rate over a predefined timescale. The model also simulates interactive ozone levels

– combined tropospheric and stratospheric – and parameterizes aerosol direct and indirect effects using logarithmic functional fits (Eqn. 8 in [14]). The sensitivity of this aerosol forcing to various species is illustrated in Supplementary Figure 9. Changes in albedo from land-use are assumed to scale linearly with cumulative AFOLU CO_2 emissions (see ref. [18] for details).

The 841-member ensemble used in this study is a subset an initial 1.6 million member ensemble sampled from AR6 probability distributions [14], chosen as follows. Each of the 1.6-million model instances has 45 free parameters. Parameters related to energy balance, the carbon cycle, ozone, and aerosol-cloud interactions are sampled from kernel-density estimates of CMIP6 results [41–44]. The other forcing parameters are sampled from IPCC AR6 ranges [45]. The resultant forcings agree closely with the extensions of the AR6 WGI estimates to present-day in the latest IGCC report (see Supplementary Figure 7). Models that fail to replicate historical global-mean surface temperatures (GMST) within a root-mean-square error (RMSE) of less than 0.2 K are excluded, eliminating 86% of the original ensemble. From the remaining models, 841 are selected that together optimally reproduce the AR6 distributions for equilibrium climate sensitivity (ECS), transient climate response (TCR), and aerosol forcing, as well as historical observations of GMST, ocean heat content, and CO_2 levels [14].

Simulations

Changes in temperature and forcing are assessed relative to their levels in 1750. The "fossil fuel" experiments are driven by the changes in emissions since preindustrial (1750) due to solely fossil-fuel activity. In these fossil-fuel experiments, emissions from non-fossil-fuel activities are held constant at their preindustrial baselines. Their inclusion is necessary to apply the aerosol forcing formulae in FaIR [14], which are tuned relative to the total pre-industrial emissions. The "other activities" experiments are likewise driven by the historical changes in the emissions since preindustrial due solely to non-fossil-fuel activities, holding fossil-fuel emissions constant at their 1750 levels.

The first set of experiments (shown in Figures 1 and 2) follow a linear projection of emissions to 2040 based on the historical growth over the last decade of each respective activity's emissions. The probability density function (PDF) shown in Figure 1 for the year when fossil-fuel activities overtake other activities as the dominant cause of global warming is computed by fitting a Gaussian kernel density (KDE) estimate with bandwidth determined by Silverman's rule [46] to the ensemble's distribution of crossing years. In Supplemental Figure 12, the cumulative distribution function is also shown.

In the second set of experiments (shown in Figure 3), historical emissions abruptly end in 2024, probing the zero-emissions commitment [33] out to 2500. We explore contrasting futures of land activity after emissions with the "no regrowth" and "full regrowth" scenarios. In the no-regrowth scenario, current levels of land activity are maintained, with no additional carbon uptake beyond the natural sinks accounted for by the FaIR model. In the full-regrowth scenario, land-use stops, allowing ecosystems to recover. This scenario adds an additional carbon sink to account for regrowth on abandoned land, removing AFOLU emissions from the atmosphere with an e-folding timescale of one century. This simple treatment of carbon uptake by soil and biomass from post-agricultural succession is relatively conservative. Over half of historical land-use emissions originate from tropical regions [47], where ecosystems typically regrow over several decades, according to biomass versus age studies of abandoned land [48]. However, we conservatively use the regrowth timescale of boreal forests, which is closer to a century, as found in studies of regrowth after disturbances [49].

Nonlinearity

Summing the total radiative forcings from the separate fossil-fuel and other-activities experiments results in a value that is 12% greater than when FaIR is driven by all emissions combined (see Table 2). The time series of this nonlinearity is displayed in Supplemental Figure 11, and computed by differencing the heating timeseries from FaIR driven by all emissions with the sum of the heating timeseries of the two separate experiments. The nonlinearity in forcing is most pronounced for methane, both directly and indirectly via its effect on ozone. Changes in methane chemistry are largely driven by NO_x [43]. As demonstrated by ESMs in ref. [43] and replicated by FaIR in Supplemental Figure 8, experiments that include fossil-fuel NO_x exhibit a $\sim$40% decline in methane's lifetime over the industrial era. Prior to this industrial era, FaIR exhibits a methane perturbation lifetime of nearly 17 years, which is higher than the 8 to 13 year range found in ESMs [14, 42].

As detailed in ref. [14], this lifetime results from an apparent inconsistency between the PRIMAP-Hist emissions, ESM sensitivity experiments, and historical concentrations of methane. FaIR accurately reproduces these concentrations and captures the ESM-inferred sensitivities of methane to other species, but does so at the expense of a realistic preindustrial lifetime. Between 1750 and 1950, FaIR's perturbation lifetime declines rapidly over time, and subsequently ranges over values within one standard deviation ($\pm$1.8 yr) of the IPCC's central estimate (11.8 yr) of methane's present-day perturbation lifetime [6].

The exaggerated lifetime in the early industrial period may be due to PRIMAP-Hist emissions underestimating the true historical values [14]. Uncertainty is also due to the inherent challenge of capturing methane chemistry with a simple parameterization, especially one that is tuned to the limited set of perturbation experiments available in AerChemMIP [43]. In light of these issues, and because the non-linear component of methane's forcing is fundamentally due to the interplay between fossil-fuel and non-fossil-fuel emissions, we attribute the nonlinearity equally to the two experiments. Thus, half of the (negative) heating due to these nonlinear effects (shown in Supplemental Figure 11) is added to the heating timeseries of the fossil-fuel and other-activities experiments. This process is repeated for each species such that the total forcing resulting from the sum of the separate experiments is scaled to match that of FaIR when driven by all emissions combined. While there are nonlinearities in the relationship between emissions and forcing, the energy-balance model in FaIR that computes the temperature from the forcings is linear.

Data Availability

Code, results, and figures are available in a Zenodo repository at https://doi.org/10.5281/zenodo.13743384.

Acknowledgments

N. Tarshish acknowledges support from an Environmental Fellowship at the Harvard University Center for the Environment. The authors thank Aaron Match, Nadir Jeevanjee, Emma Ignaszewski, and Andrew Williams for their valuable feedback on an earlier version of this work.

References

[1] Jay, A.K., Crimmins, A.R., Avery, C.W., Dahl, T.A., Dodder, R.S., Hamlington, B.D., Lustig, A., Marvel, K., Méndez-Lazaro, P.A., Osler, M.S., Terando, A., Weeks, E.S., Zycherman, A.: Chapter 1: Overview. Fifth National Climate Assessment (2023). https://doi.org/10.7930/NCA5.2023.CH1

[2] U.S. Environmental Protection Agency: Causes of Climate Change. Accessed: 2024-06-14 (2024). https://www.epa.gov/climatechange-science/causes-climate-change

[3] NASA: Scientific Consensus: Earth's Climate is Warming. Accessed: 2024-06-14 (2024). https://science.nasa.gov/climate-change/scientific-consensus/

[4] United Nations: What is Climate Change? Accessed: 2024-06-14 (2024). https://www.un.org/sites/un2.un.org/files/fastfacts-what-is-climate-change.pdf

[5] IPCC: Summary for policymakers. In: Masson-Delmotte, V., Zhai, P., Pirani, A., Connors, S.L., Péan, C., Berger, S., Caud, N., Chen, Y., Goldfarb, L., Gomis, M.I., Huang, M., Leitzell, K., Lonnoy, E., Matthews, J.B.R., Maycock, T.K., Waterfield, T., Yelekçi, O., Yu, R., Zhou, B. (eds.) Climate Change 2021: The Physical Science Basis. Contribution of Working Group I to the Sixth Assessment Report of the Intergovernmental Panel on Climate Change, pp. 1–31. Cambridge University Press, Cambridge, UK and New York, NY, USA (2021). https://doi.org/10.1017/9781009157896.001

[6] Szopa, S., Naik, V., Adhikary, B., Artaxo, P., Berntsen, T., Collins, W.D., Fuzzi, S., Gallardo, L., Kiendler-Scharr, A., Klimont, Z., Liao, H., Unger, N., Zanis, P.: Short-lived climate forcers. In: Masson-Delmotte, V., Zhai, P., Pirani, A., Connors, S.L., Péan, C., Berger, S., Caud, N., Chen, Y., Goldfarb, L., Gomis, M.I., Huang, M., Leitzell, K., Lonnoy, E., Matthews, J.B.R., Maycock, T.K., Waterfield, T., Yelekçi, O., Yu, R., Zhou, B. (eds.) Climate Change 2021: The Physical Science Basis. Contribution of Working Group I to the Sixth Assessment Report of the Intergovernmental Panel on Climate Change, pp. 817–921. Cambridge University Press, Cambridge, UK and New York, NY, USA (2021). Chap. 6. https://doi.org/10.1017/9781009157896.008

[7] Wigley, T.M.L.: Possible climate change due to SO_2-derived cloud condensation nuclei. Nature **339**, 365–367 (1989) https://doi.org/10.1038/339365a0

[8] Hansen, J., Rossow, W., Fung, I.: The missing data on global climate change. Issues in Science and Technology **7**(1), 62–69 (1990)

[9] Charlson, R.J., Schwartz, S., Hales, J., Cess, R.D., Coakley Jr, J., Hansen, J., Hofmann, D.: Climate forcing by anthropogenic aerosols. Science **255**(5043), 423–430 (1992)

[10] Mitchell, J.F.B., Johns, T.C., Gregory, J.M., Tett, S.F.B.: Climate response to increasing levels of greenhouse gases and sulphate aerosols. Nature **376**, 501–504 (1995) https://doi.org/10.1038/376501a0

[11] Forster, P.M., Smith, C., Walsh, T., Lamb, W.F., Lamboll, R., Hall, B., Hauser, M., Ribes, A., Rosen, D., Gillett, N.P., Palmer, M.D., Rogelj, J., Schuckmann, K., Trewin, B., Allen, M., Andrew, R., Betts, R.A., Borger, A., Boyer, T., Broersma, J.A., Buontempo, C., Burgess, S., Cagnazzo, C., Cheng, L., Friedlingstein, P., Gettelman, A., Gütschow, J., Ishii, M., Jenkins, S., Lan, X., Morice, C., Mühle, J., Kadow, C., Kennedy, J., Killick, R.E., Krummel, P.B., Minx, J.C., Myhre, G., Naik, V., Peters, G.P., Pirani, A., Pongratz, J., Schleussner, C.-F., Seneviratne, S.I., Szopa, S., Thorne, P., Kovilakam, M.V.M., Majamäki, E., Jalkanen, J.-P., Marle, M., Hoesly, R.M., Rohde, R., Schumacher, D., Werf, G., Vose, R., Zickfeld, K., Zhang, X., Masson-Delmotte, V., Zhai, P.: Indicators of Global Climate Change 2023: annual update of key indicators of the state of the climate system and human influence. Earth System Science Data **16**(6), 2625–2658 (2024) https://doi.org/10.5194/essd-16-2625-2024

[12] Shindell, D., Faluvegi, G.: The net climate impact of coal-fired power plant emissions. Atmospheric Chemistry and Physics **10**(7), 3247–3260 (2010) https://doi.org/10.5194/acp-10-3247-2010

[13] Dreyfus, G.B., Xu, Y., Shindell, D.T., Zaelke, D., Ramanathan, V.: Mitigating climate disruption in time: A self-consistent approach for avoiding both near-term and long-term global warming. Proceedings of the National Academy of Sciences **119**(22), 2123536119 (2022)

[14] Smith, C., Cummins, D.P., Fredriksen, H.-B., Nicholls, Z., Meinshausen, M., Allen, M., Jenkins, S., Leach, N., Mathison, C., Partanen, A.-I.: fair-calibrate v1.4.1: calibration, constraining and validation of the FaIR simple climate model for reliable future climate projections. EGUsphere **2024**, 1–36 (2024) https://doi.org/10.5194/egusphere-2024-708

[15] Myhre, G., Shindell, D., Bréon, F.-M., Collins, W., Fuglestvedt, J., Huang, J., Koch, D., Lamarque, J.-F., Lee, D., Mendoza, B., Nakajima, T., Robock, A., Stephens, G., Takemura, T., Zhang, H.: 8. In: Stocker, T.F., Qin, D., Plattner, G.-K., Tignor, M., Allen, S.K., Boschung, J., Nauels, A., Xia, Y., Bex, V., Midgley, P.M. (eds.) Anthropogenic and Natural Radiative Forcing, pp. 659–740. Cambridge University Press, Cambridge, United Kingdom and New York, NY, USA (2013). https://doi.org/10.1017/CBO9781107415324.018

[16] Masson-Delmotte, V., Zhai, P., Pörtner, H.-O., Roberts, D., Skea, J., Shukla, P.R., Pirani, A., Moufouma-Okia, W., Péan, C., Bojariu, R., Connors, S., Bethke, J., Matthews, R., Chen, Y., Zhou, X., Gomis, M.I., Lonnoy, E., Maycock, T., Tignor, M., Waterfield, T. (eds.): Global Warming of 1.5°C. An IPCC Special Report on the Impacts of Global Warming of 1.5°C Above Pre-industrial Levels and Related Global Greenhouse Gas Emission Pathways, in the Context of Strengthening the Global Response to the Threat of Climate Change, Sustainable Development, and Efforts to Eradicate Poverty, p. 616. Cambridge University Press, Cambridge, UK and New York, NY, USA (2018). https://doi.org/10.1017/9781009157940

[17] Forster, P., Storelvmo, T., Armour, K., Collins, W., Dufresne, J.-L., Frame, D., Lunt, D.J., Mauritsen, T., Palmer, M.D., Watanabe, M., Wild, M., Zhang, H.: The earth's energy budget, climate feedbacks, and climate sensitivity supplementary material. In: Masson-Delmotte, V., Zhai, P., Pirani, A., Connors, S.L., Péan, C., Berger, S., Caud, N., Chen, Y., Goldfarb, L., Gomis, M.I., Huang, M., Leitzell, K., Lonnoy, E., Matthews, J.B.R., Maycock, T.K., Waterfield, T., Yelekçi, O., Yu, R., Zhou, B. (eds.) Climate Change 2021: The Physical Science Basis. Contribution of Working Group I to the Sixth Assessment Report of the Intergovernmental Panel on Climate Change, pp. 1–35. Cambridge University Press, Cambridge, UK and New York, NY, USA (2021)

[18] Smith, C.J., Forster, P.M., Allen, M., Leach, N., Millar, R.J., Passerello, G.A., Regayre, L.A.: FAIR v1.3: a simple emissions-based impulse response and carbon cycle model. Geoscientific Model Development **11**, 2273–2297 (2018) https://doi.org/10.5194/gmd-11-2273-2018

[19] Nicholls, Z.R.J., Meinshausen, M., Lewis, J., Gieseke, R., Dommenget, D., Dorheim, K., Fan, C.-S., Fuglestvedt, J.S., Gasser, T., Golüke, U., Goodwin, P., Hartin, C., Hope, A.P., Kriegler, E., Leach,

N.J., Marchegiani, D., McBride, L.A., Quilcaille, Y., Rogelj, J., Salawitch, R.J., Samset, B.H., Sandstad, M., Shiklomanov, A.N., Skeie, R.B., Smith, C.J., Smith, S., Tanaka, K., Tsutsui, J., Xie, Z.: Reduced Complexity Model Intercomparison Project Phase 1: introduction and evaluation of global-mean temperature response. Geoscientific Model Development **13**(11), 5175–5190 (2020) https://doi.org/10.5194/gmd-13-5175-2020

[20] Leach, N.J., Jenkins, S., Nicholls, Z., Smith, C.J., Lynch, J., Cain, M., Walsh, T., Wu, B., Tsutsui, J., Allen, M.R.: FaIRv2.0.0: a generalized impulse response model for climate uncertainty and future scenario exploration. Geoscientific Model Development **14**(5), 3007–3036 (2021)

[21] Marle, M.J.E., Kloster, S., Magi, B.I., Marlon, J.R., Daniau, A.-L., Field, R.D., Arneth, A., Forrest, M., Hantson, S., Kehrwald, N.M., *et al.*: Historic global biomass burning emissions for CMIP6 (BB4CMIP) based on merging satellite observations with proxies and fire models (1750–2015). Geoscientific Model Development **10**, 3329–3357 (2017) https://doi.org/10.5194/gmd-10-3329-2017

[22] Hoesly, R.M., Smith, S.J., Feng, L., Klimont, Z., Janssens-Maenhout, G., Pitkanen, T., Seibert, J.J., Vu, L., Andres, R.J., Bolt, R.M., *et al.*: Historical (1750–2014) anthropogenic emissions of reactive gases and aerosols from the Community Emissions Data System (CEDS). Geoscientific Model Development **11**, 369–408 (2018) https://doi.org/10.5194/gmd-11-369-2018

[23] Gütschow, J., Jeffery, M.L., Gieseke, R., Gebel, R., Stevens, D., Krapp, M., Rocha, M.: The PRIMAP-hist national historical emissions time series. Earth Syst. Sci. Data **8**, 571–603 (2016) https://doi.org/10.5194/essd-8-571-2016

[24] Werf, G.R., Randerson, J.T., Giglio, L., Leeuwen, T.T., Chen, Y., Rogers, B.M., Mu, M., Marle, M.J.E., Morton, D.C., Collatz, G.J., Yokelson, R.J., Kasibhatla, P.S.: Global fire emissions estimates during 1997–2016. Earth Syst. Sci. Data **9**, 697–720 (2017) https://doi.org/10.5194/essd-9-697-2017

[25] Friedlingstein, P., *et al.*: Global Carbon Budget 2023. Earth Syst. Sci. Data **15**, 5301–5369 (2023) https://doi.org/10.5194/essd-15-5301-2023

[26] Hoesly, R., Smith, S.: CEDS v2024-04-01 Release Emission Data. Zenodo (2024). https://doi.org/10.5281/zenodo.10904361

[27] Liu, F., Choi, S., Li, C., Fioletov, V.E., McLinden, C.A., Joiner, J., Krotkov, N.A., Bian, H., Janssens-Maenhout, G., Darmenov, A.S., Silva, A.M.: A new global anthropogenic SO_2 emission inventory for the last decade: a mosaic of satellite-derived and bottom-up emissions. Atmospheric Chemistry and Physics **18**(22), 16571–16586 (2018) https://doi.org/10.5194/acp-18-16571-2018

[28] Intergovernmental Panel on Climate Change: 2019 Refinement to the 2006 IPCC Guidelines for National Greenhouse Gas Inventories. https://www.ipcc-nggip.iges.or.jp/public/2019rf/index.html (2019). https://doi.org/10.1016/j.jclepro.2020.122231

[29] Nabuurs, G.-J., Mrabet, R., Hatab, A.A., Bustamante, M., Clark, H., Havlík, P., House, J., Mbow, C., Ninan, K.N., Popp, A., Roe, S., Sohngen, B., Towprayoo, S.: Agriculture, forestry and other land uses (afolu). In: Shukla, P.R., Skea, J., Slade, R., Khourdajie, A.A., Diemen, R., McCollum, D., Pathak, M., Some, S., Vyas, P., Fradera, R., Belkacemi, M., Hasija, A., Lisboa, G., Luz, S., Malley, J. (eds.) Climate Change 2022: Mitigation of Climate Change. Contribution of Working Group III to the Sixth Assessment Report of the Intergovernmental Panel on Climate Change. Cambridge University Press, Cambridge, UK and New York, NY, USA (2022). https://doi.org/10.1017/9781009157926.009

[30] Archer, D., Kheshgi, H., Maier-Reimer, E.: Multiple timescales for neutralization of fossil fuel CO_2. Geophysical Research Letters **24**(4), 405–408 (1997)

[31] Matthews, H.D., Caldeira, K.: Stabilizing climate requires near-zero emissions. Geophysical Research Letters **35**(4) (2008) https://doi.org/10.1029/2007GL032388

[32] Solomon, S., Plattner, G.-K., Knutti, R., Friedlingstein, P.: Irreversible climate change due to carbon dioxide emissions. Proceedings of the National Academy of Sciences **106**(6), 1704–1709 (2009)

[33] Palazzo Corner, S., Siegert, M., Ceppi, P., Fox-Kemper, B., Frölicher, T.L., Gallego-Sala, A., Haigh, J., Hegerl, G.C., Jones, C.D., Knutti, R., Koven, C.D., MacDougall, A.H., Meinshausen, M., Nicholls, Z., Sallée, J.B., Sanderson, B.M., Séférian, R., Turetsky, M., Williams, R.G., Zaehle, S., Rogelj, J.: The Zero Emissions Commitment and climate stabilization. Frontiers in Science **1** (2023) https://doi.org/10.3389/fsci.2023.1170744

[34] International Energy Agency: World energy outlook 2023. Technical report, International Energy Agency (2023). https://doi.org/10.1787/af34e39f-en

[35] Riahi, K., Vuuren, D.P., *et al.*: The shared socioeconomic pathways and their energy, land use, and greenhouse gas emissions implications: An overview. Global Environmental Change **42**, 153–168 (2017) https://doi.org/10.1016/j.gloenvcha.2016.05.009

[36] Friedlingstein, P., *et al.*: Global carbon budget 2023. Earth System Science Data **15**, 5301–5369 (2023) https://doi.org/10.5194/essd-15-5301-2023

[37] Lamboll, R.D., Jones, C.D., Skeie, R.B., Fiedler, S., Samset, B.H., Gillett, N.P., Rogelj, J., Forster, P.M.: Modifying emissions scenario projections to account for the effects of COVID-19: protocol for CovidMIP. Geoscientific Model Development **14**, 3683–3695 (2021) https://doi.org/10.5194/gmd-14-3683-2021

[38] Gütschow, J., Pflüger, M.: The PRIMAP-hist national historical emissions time series (1750-2022) v2.5. Zenodo (2023). https://doi.org/10.5281/zenodo.10006301 . https://doi.org/10.5281/zenodo.10006301

[39] IPCC: Scenarios and modelling methods. In: Guivarch, C., Kriegler, E., Portugal-Pereira, J., Bosetti, V., Edmonds, J., Fischedick, M., Havlík, P., Jaramillo, P., Krey, V., Lecocq, F., Lucena, A., Meinshausen, M., Mirasgedis, S., O'Neill, B., Peters, G.P., Rogelj, J., Rose, S., Saheb, Y., Strbac, G., Hammer Strømman, A., Vuuren, D.P., Zhou, N. (eds.) Climate Change 2022: Mitigation of Climate Change. Contribution of Working Group III to the Sixth Assessment Report of the Intergovernmental Panel on Climate Change. Cambridge University Press, Cambridge, UK and New York, NY, USA (2022). https://doi.org/10.1017/9781009157926.022

[40] Millar, R.J., Nicholls, Z.R., Friedlingstein, P., Allen, M.R.: A modified impulse-response representation of the global near-surface air temperature and atmospheric concentration response to carbon dioxide emissions. Atmospheric Chemistry and Physics **17**, 7213–7228 (2017) https://doi.org/10.5194/acp-17-7213-2017

[41] Skeie, R.B., Myhre, G., Hodnebrog, Ø., Cameron-Smith, P.J., Deushi, M., Hegglin, M.I., Horowitz, L.W., Kramer, R.J., Michou, M., Mills, M.J., Olivié, D.J.L., O'Connor, F.M., Paynter, D., Samset, B.H., Sellar, A., Shindell, D., Takemura, T., Tilmes, S., Wu, T.: Historical total ozone radiative forcing derived from CMIP6 simulations. npj Climate and Atmospheric Science **3**, 32 (2020) https://doi.org/10.1038/s41612-020-00131-0

[42] Thornhill, G., Collins, W., Olivié, D., Skeie, R.B., Archibald, A., Bauer, S., Checa-Garcia, R., Fiedler, S., Folberth, G., Gjermundsen, A., Horowitz, L., Lamarque, J.-F., Michou, M., Mulcahy, J., Nabat, P., Naik, V., O'Connor, F.M., Paulot, F., Schulz, M., Scott, C.E., Séférian, R., Smith, C., Takemura, T., Tilmes, S., Tsigaridis, K., Weber, J.: Climate-driven chemistry and aerosol feedbacks in CMIP6 earth system models **21**, 1105–1126 (2021) https://doi.org/10.5194/acp-21-1105-2021

[43] Thornhill, G.D., Collins, W.J., Kramer, R.J., Olivié, D., Skeie, R.B., O'Connor, F.M., Abraham, N.L., Checa-Garcia, R., Bauer, S.E., Deushi, M., Emmons, L.K., Forster, P.M., Horowitz, L.W., Johnson, B., Keeble, J., Lamarque, J.-F., Michou, M., Mills, M.J., Mulcahy, J.P., Myhre, G., Nabat, P., Naik, V., Oshima, N., Schulz, M., Smith, C.J., Takemura, T., Tilmes, S., Wu, T., Zeng, G., Zhang, J.: Effective radiative forcing from emissions of reactive gases and aerosols – a multi-model comparison. Atmospheric Chemistry and Physics **21**, 853–874 (2021) https://doi.org/10.5194/acp-21-853-2021

[44] Arora, V.K., Katavouta, A., Williams, R.G., Jones, C.D., Brovkin, V., Friedlingstein, P., Schwinger, J., Bopp, L., Boucher, O., Cadule, P., *et al.*: Carbon–concentration and carbon–climate feedbacks in CMIP6 models and their comparison to CMIP5 models. Biogeosciences **17**, 4173–4222 (2020) https://doi.org/10.5194/bg-17-4173-2020

[45] Lee, J.-Y., Marotzke, J., Bala, G., Cao, L., Corti, S., Dunne, J., Engelbrecht, F., Fischer, E., Fyfe, J., Jones, C., Maycock, A., Mutemi, J., Ndiaye, O., Panickal, S., Zhou, T.: In: Masson-Delmotte, V., Zhai, P., Pirani, A., Connors, S.L., Péan, C., Berger, S., Caud, N., Chen, Y., Goldfarb, L. (eds.) Future Global Climate: Scenario-Based Projections and Near-Term Information. Intergovernmental Panel on Climate Change, Geneva, Switzerland (2021)

[46] Silverman, B.W.: Density Estimation for Statistics and Data Analysis, p. 45. Chapman & Hall/CRC, London (1986)

[47] Houghton, R.A., Castanho, A.: Annual emissions of carbon from land use, land-use change, and forestry from 1850 to 2020. Earth System Science Data **15**(5), 2025–2054 (2023) https://doi.org/10.5194/essd-15-2025-2023

[48] Marìn-Spiotta, E., Cusack, D.F., Ostertag, R., Silver, W.L.: Trends in Above and Belowground Carbon with Forest Regrowth After Agricultural Abandonment in the Neotropics, pp. 22–72. Springer, New York, NY (2008). https://doi.org/10.1007/978-0-387-33642-8

[49] Tompalski, P., Wulder, M.A., White, J.C., Hermosilla, T., Riofrío, J., Kurz, W.A.: Developing aboveground biomass yield curves for dominant boreal tree species from time series remote sensing data. Forest Ecology and Management **561**, 121894 (2024)

Supplemental Materials

Table 1: Assignment of CEDS [22] subsectors to fossil fuels and other activities. In the main figures, the ambiguous column is grouped with the other activities. Supplementary Figure 12 demonstrates the impact of alternatively associating these ambiguous emissions with fossil fuels.

Fossil Fuels	**Other**	**Ambiguous**
1A1a_Electricity-autoproducer	2A1_Cement-production	2Ax_Other-minerals
1A1a_Electricity-public	2A2_Lime-production	2B2_Chemicals-Nitric-acid
1A1a_Heat-production	3B_Manure-management	2B3_Chemicals-Adipic-acid
1A1bc_Other-transformation	3D_Rice-Cultivation	2B_Chemical-industry
1A2a_Ind-Comb-Iron-steel	3D_Soil-emissions	2D_Chemical-products-manufacture-processing
1A2b_Ind-Comb-Non-ferrous-metals	3E_Enteric-fermentation	2D_Degreasing-Cleaning
1A2c_Ind-Comb-Chemicals	3F_Agricultural-residue-burning-on-fields	2D_Other-product-use
1A2d_Ind-Comb-Pulp-paper	3I_Agriculture-other	2D_Paint-application
1A2e_Ind-Comb-Food-tobacco	5A_Solid-waste-disposal	2H_Pulp-and-paper-food-beverage-wood
1A2f_Ind-Comb-Non-metalic-minerals	5D_Wastewater-handling	2L_Other-process-emissions
1A2g_Ind-Comb-Construction	5E_Other-waste-handling	
1A2g_Ind-Comb-machinery		
1A2g_Ind-Comb-mining-quarying		
1A2g_Ind-Comb-other		
1A2g_Ind-Comb-textile-leather		
1A2g_Ind-Comb-transpequip		
1A2g_Ind-Comb-wood-products		
1A3ai_International-aviation		
1A3aii_Domestic-aviation		
1A3b_Road		
1A3c_Rail		
1A3di_International-shipping		
1A3di_Oil_Tanker_Loading		
1A3di_Oil_tanker_loading		
1A3dii_Domestic-navigation		
1A3eii_Other-transp		
1A4a_Commercial-institutional		
1A4b_Residential		
1A4c_Agriculture-forestry-fishing		
1A5_Other-unspecified		
1B1_Fugitive-solid-fuels		
1B2_Fugitive-petr		
1B2_Fugitive-petr-and-gas		
1B2b_Fugitive-NG-distr		
1B2b_Fugitive-NG-prod		
1B2d_Fugitive-other-energy		
2C_Metal-production		
5C_Waste-combustion		
6A_Other-in-total		
6B_Other-not-in-total		
7A_Fossil-fuel-fires		
7BC_Indirect-N2O-non-agricultural-N		

Table 2: Effective radiative forcing from 1750 to 2023. The latest radiative forcings estimates by the IGCC [11] are compared to the FaIR ensemble driven by all emissions, fossil fuels, and other activities. The second column differs from the sum of the third and fourth columns due to nonlinearities in FaIR (see Supplemental Figure 11). Median and 5th-95th interquantile ranges are shown.

Forcing	IGCC	FaIR	FaIR: Fossil Fuels	FaIR: Other Activities
Anthropogenic	2.91 (2.17/3.62)	2.88 (2.29/3.46)	1.47 (1.07/1.90)	1.76 (1.29/2.16)
CO_2	2.25 (1.98/2.52)	2.25 (1.98/2.52)	1.58 (1.38/1.79)	0.75 (0.65/0.85)
CH_4	0.56 (0.45/0.67)	0.58 (0.47/0.69)	0.27 (0.21/0.32)	0.55 (0.44/0.66)
N_2O	0.22 (0.19/0.25)	0.22 (0.18/0.24)	0.04 (0.03/0.04)	0.19 (0.16/0.21)
Aerosols	-0.97 (-1.59/-0.39)	-0.93 (-1.54/-0.41)	-0.73 (-1.10/-0.32)	-0.25 (-0.77/-0.03)
Aerosol-cloud	-0.77 (-1.35/-0.23)	-0.73 (-1.33/-0.26)	-0.55 (-0.93/-0.19)	-0.23 (-0.76/-0.02)
Aerosol-radiation	-0.20 (-0.41/0.01)	-0.20 (-0.40/0.01)	-0.18 (-0.35/0.01)	-0.03 (-0.08/0.03)
O_3	0.48 (0.24/0.71)	0.45 (0.22/0.65)	0.26 (0.12/0.39)	0.28 (0.14/0.43)
Halogenated Gases	0.41 (0.33/0.49)	0.41 (0.33/0.48)	0.00 (0.00/0.00)	0.41 (0.33/0.48)
Land-use albedo	-0.20 (-0.30/-0.10)	-0.20 (-0.30/-0.09)	0.00 (0.00/0.00)	-0.20 (-0.30/-0.09)
Particles on snow + ice	0.07 (-0.00/0.16)	0.06 (-0.00/0.14)	0.04 (-0.00/0.08)	0.03 (-0.00/0.06)
Stratospheric water vapor	0.05 (-0.00/0.10)	0.05 (0.00/0.11)	0.03 (0.00/0.05)	0.05 (0.00/0.11)

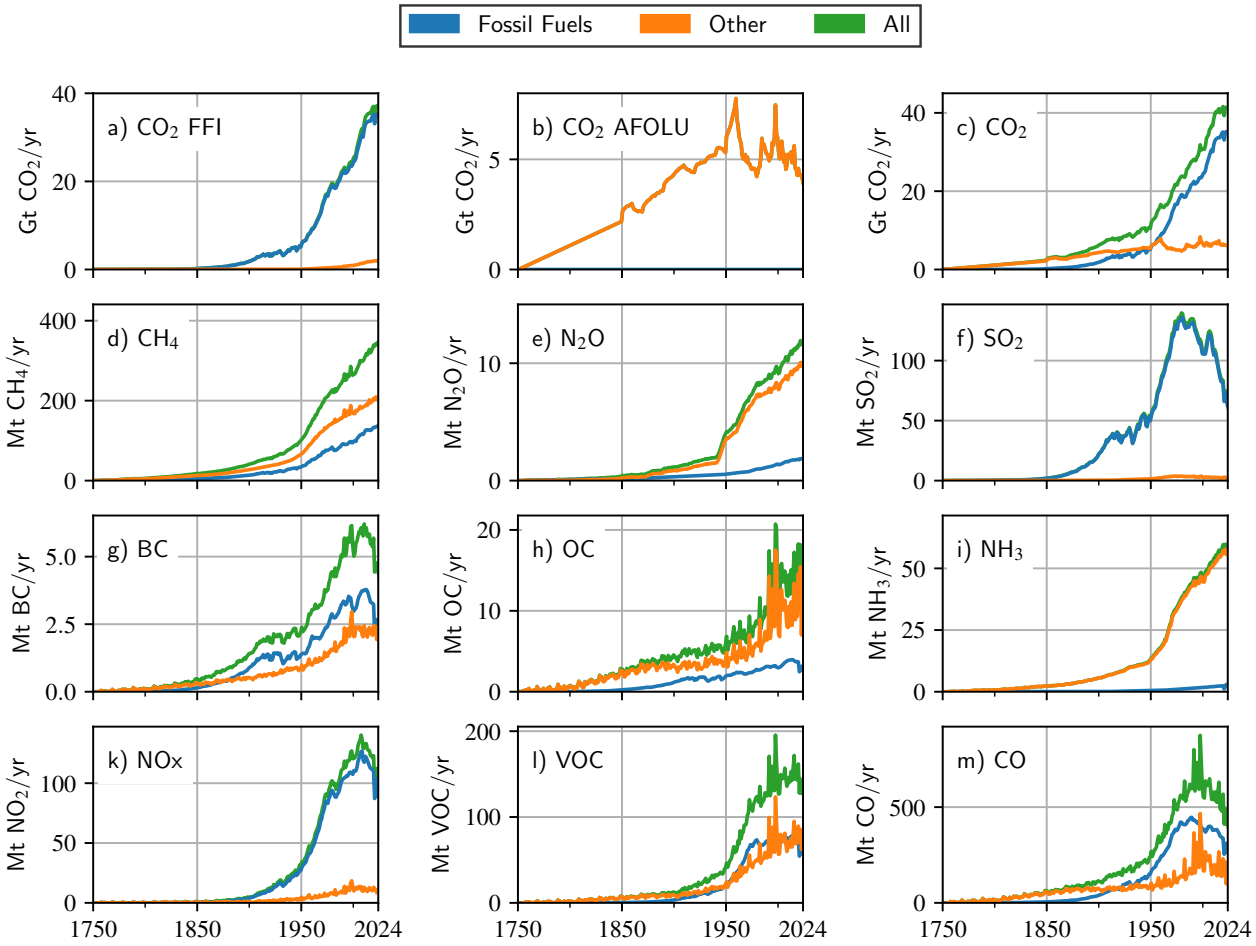

Fig. 4: The change in emissions from preindustrial due to fossil-fuel activities (blue), other activities (orange), and all activities combined (green) for various species. The changes due to all activities are identical to the results of ref. [14]. For CO_2, fossil-fuel and industrial emissions (FFI) are separated from agriculture, forestry, and land use (AFOLU) emissions.

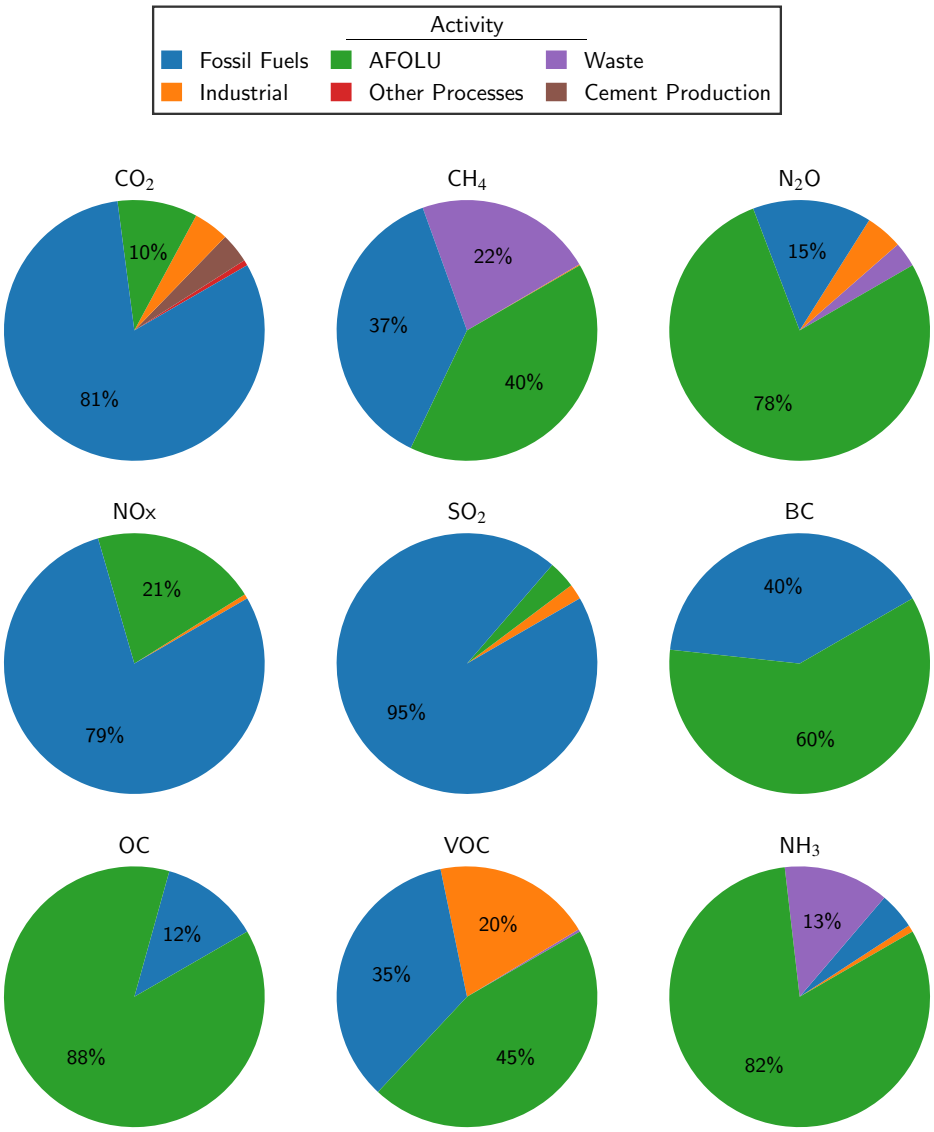

Fig. 5: The fractional contribution of different activities to the emissions of key species in 2022. Here, the blue "Fossil Fuels" activity encompasses all fossil-fuel emissions. Note that AFOLU here includes emissions from open biomass burning (GFED) and biomass combustion for energy purposes (CEDS).

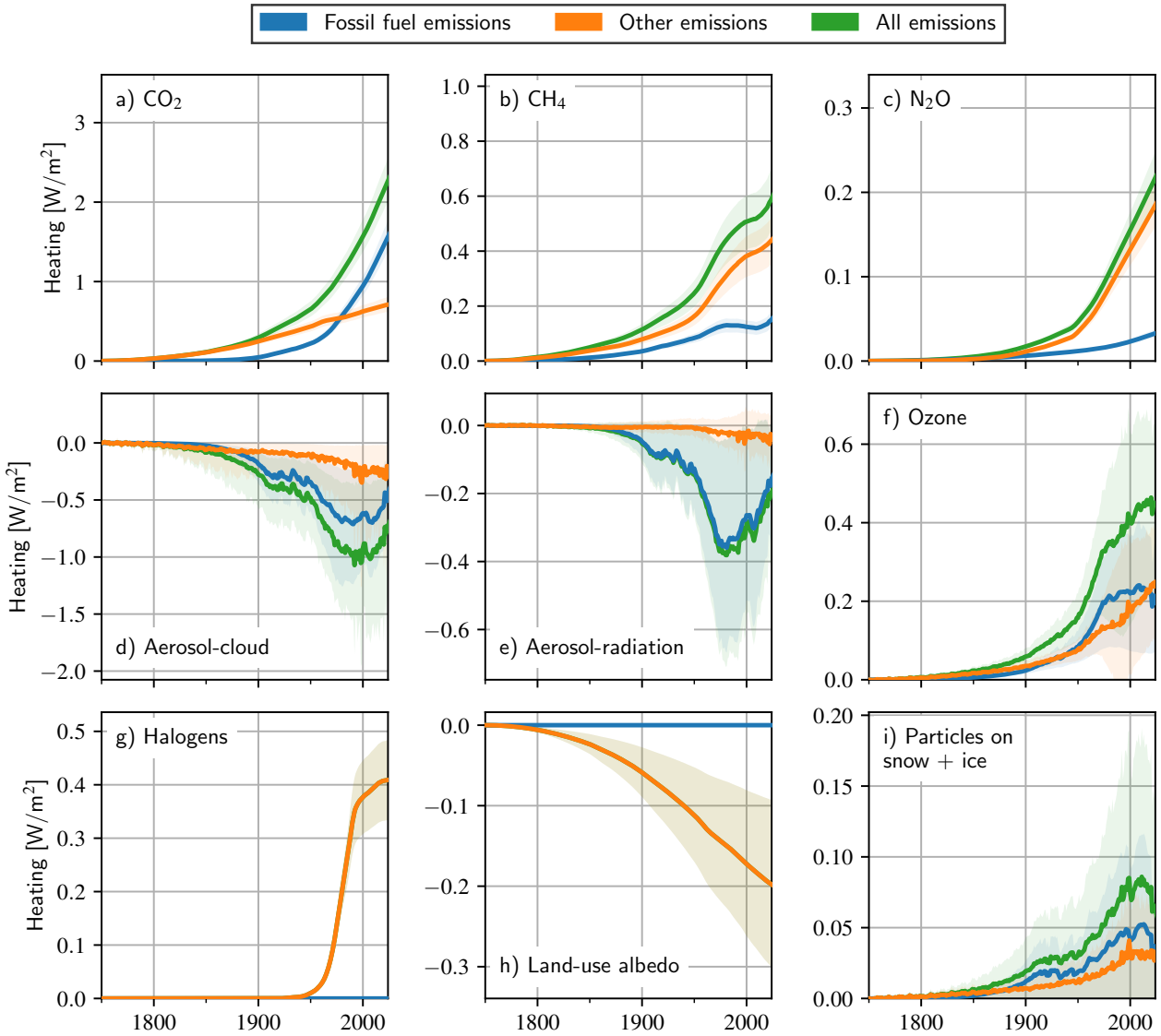

Fig. 6: Effective radiative forcings computed by the FaIR ensemble given the change in emissions since preindustrial due to all activities (green), solely fossil fuels (blue), and other activities (green). Solid lines are median estimates and shading represents the 5th-95th interquantile range.

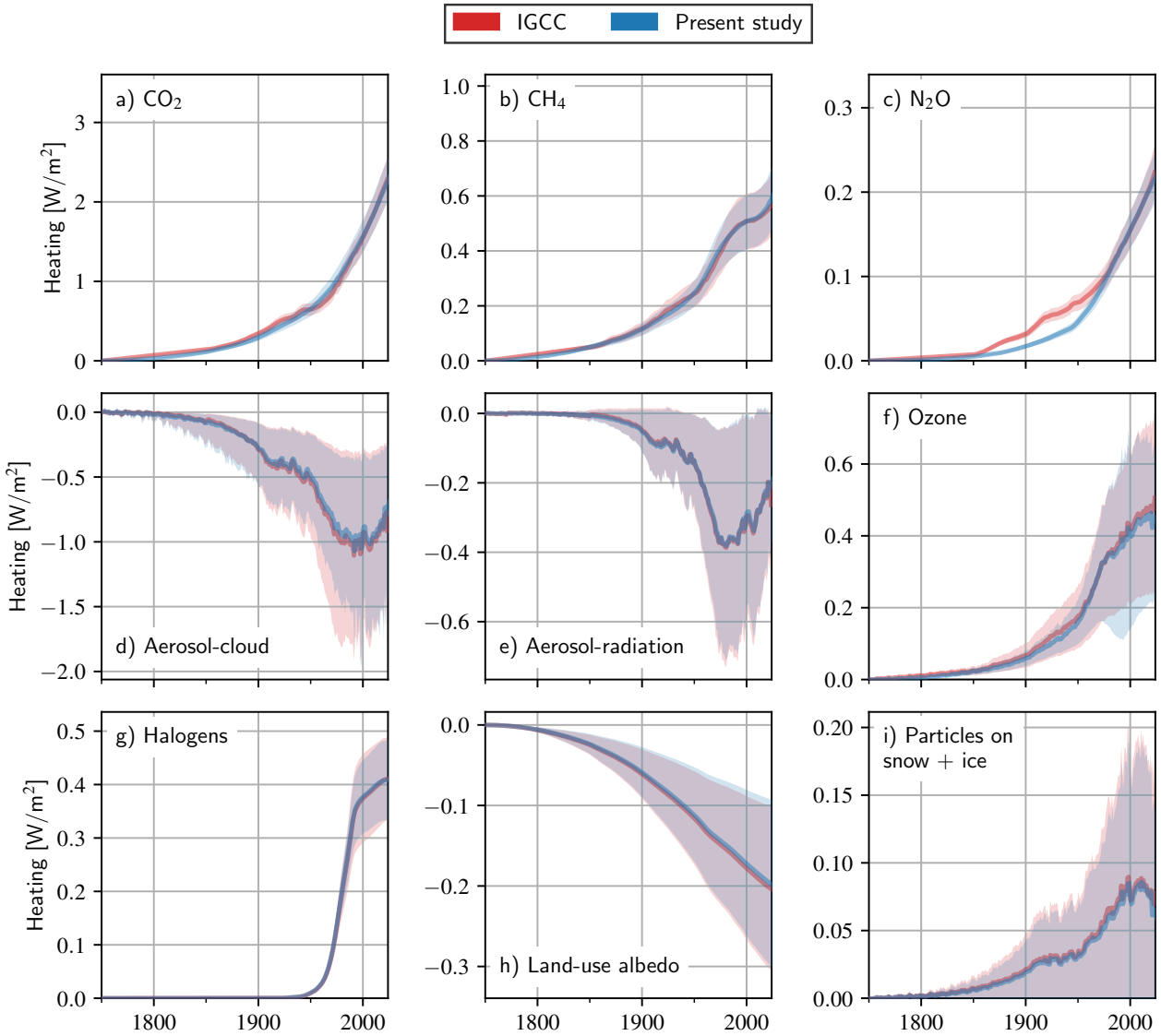

Fig. 7: Effective radiative forcing (ERF) computed by the FaIR ensemble given all historical emissions (blue) compared to the IGCC estimates (red) for various species. Solid lines are median estimates and shading represents the 5th-95th interquantile range. The IGCC estimates [11] extend the AR6 WGI ERF forcing timeseries given the most recent concentrations. Close agreement is found with the FaIR model because the FaIR forcing parameters are calibrated to the AR6 assessed ranges.

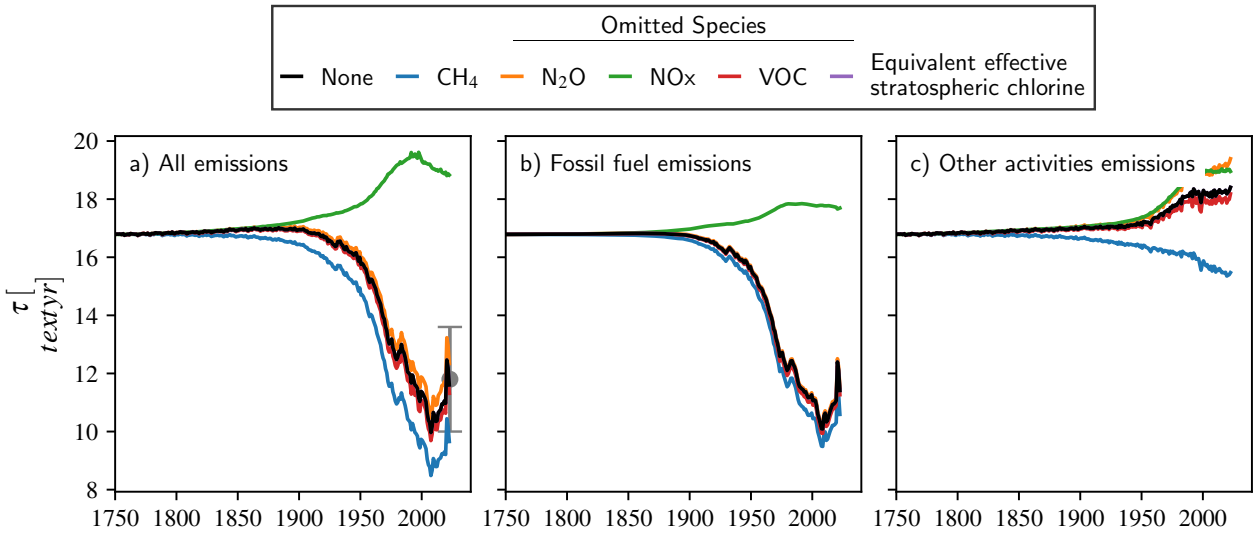

Fig. 8: The sensitivity of methane's lifetime (τ) to various species illustrated through a series of FaIR perturbation experiments. Each experiment computes the change in the perturbation lifetime of methane by holding the emissions of one species at preindustrial levels while allowing others to follow historical trends. The curves are labeled according to the species whose emissions are held fixed to preindustrial. Marker and bars indicate the central estimate and standard deviation, respectively, as assessed in AR6 [6].

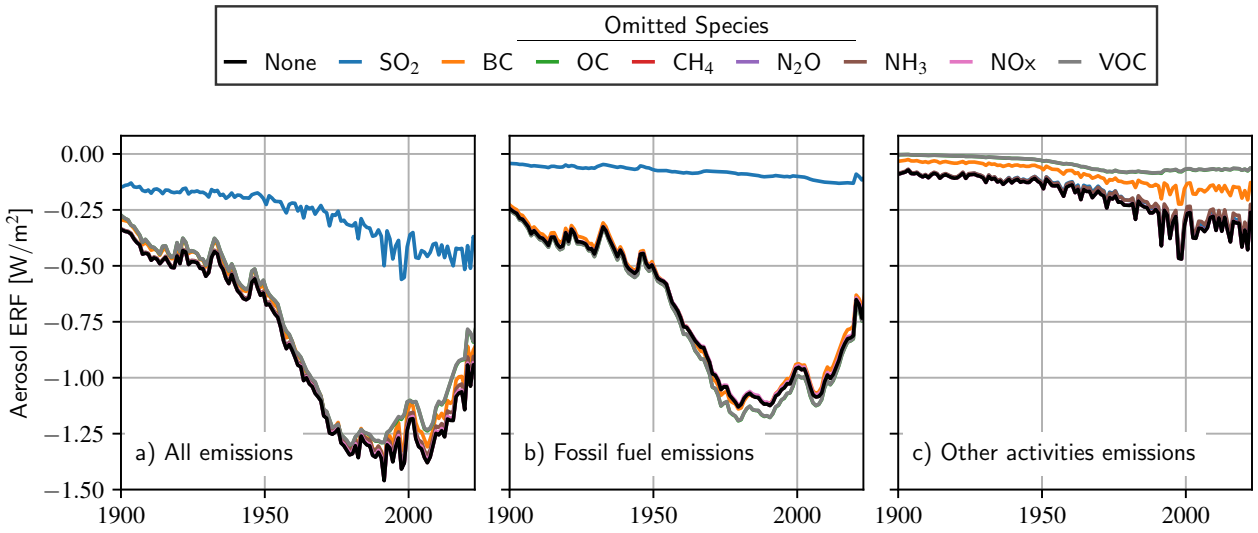

Fig. 9: Same as Figure 8 but for the total effective radiative forcing (ERF) due to aerosols.

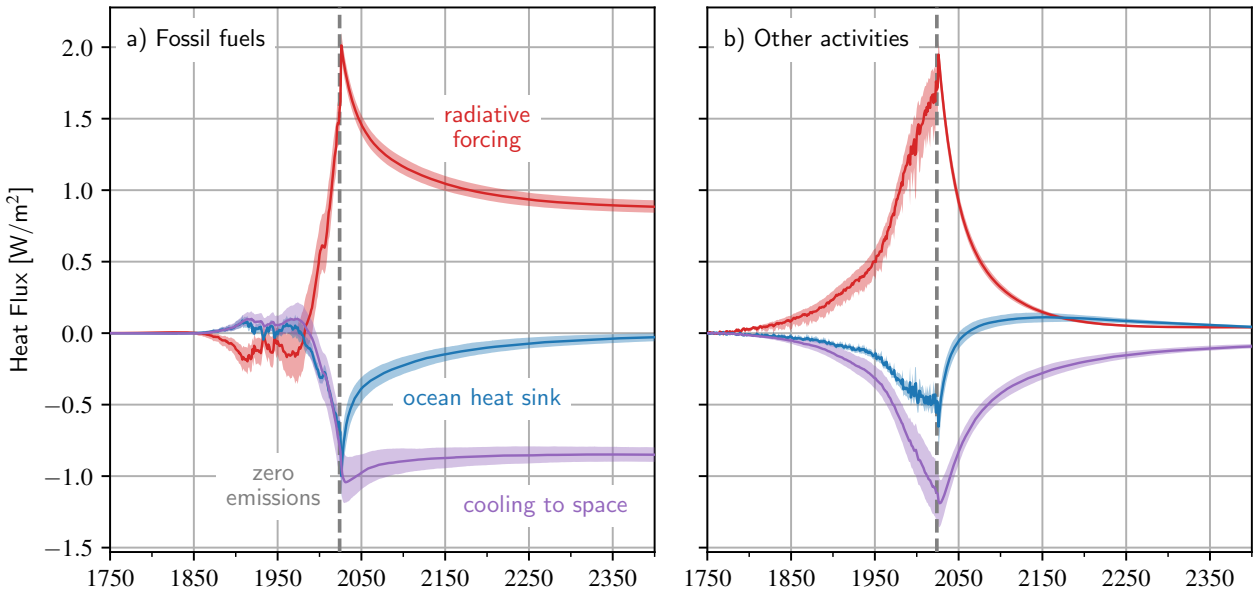

Fig. 10: Heat fluxes contributing to the surface energy anomaly budget in the FaIR abrupt-cessation experiments given historical fossil-fuel emissions (a) and other activities (b), respectively. The later experiment includes full ecosystem regrowth after AFOLU activities cease. After fossil-fuel emissions (a) end, the decline in radiative forcing (red) by roughly 1 W/m^2 is compensated for by a decrease in cooling to the deep ocean (blue) of equal magnitude. The surface temperature, which is proportional to the cooling to space (purple) in FaIR, exhibits a post-emissions plateau due to this cancellation. In the other activities experiment, uptake of AFOLU CO_2 given regrowth along with the disappearance of short-lived forcings results in a negligible forcing on multi-centennial timescales, yielding a dramatic temperature decline. Shading indicates interquartile range.

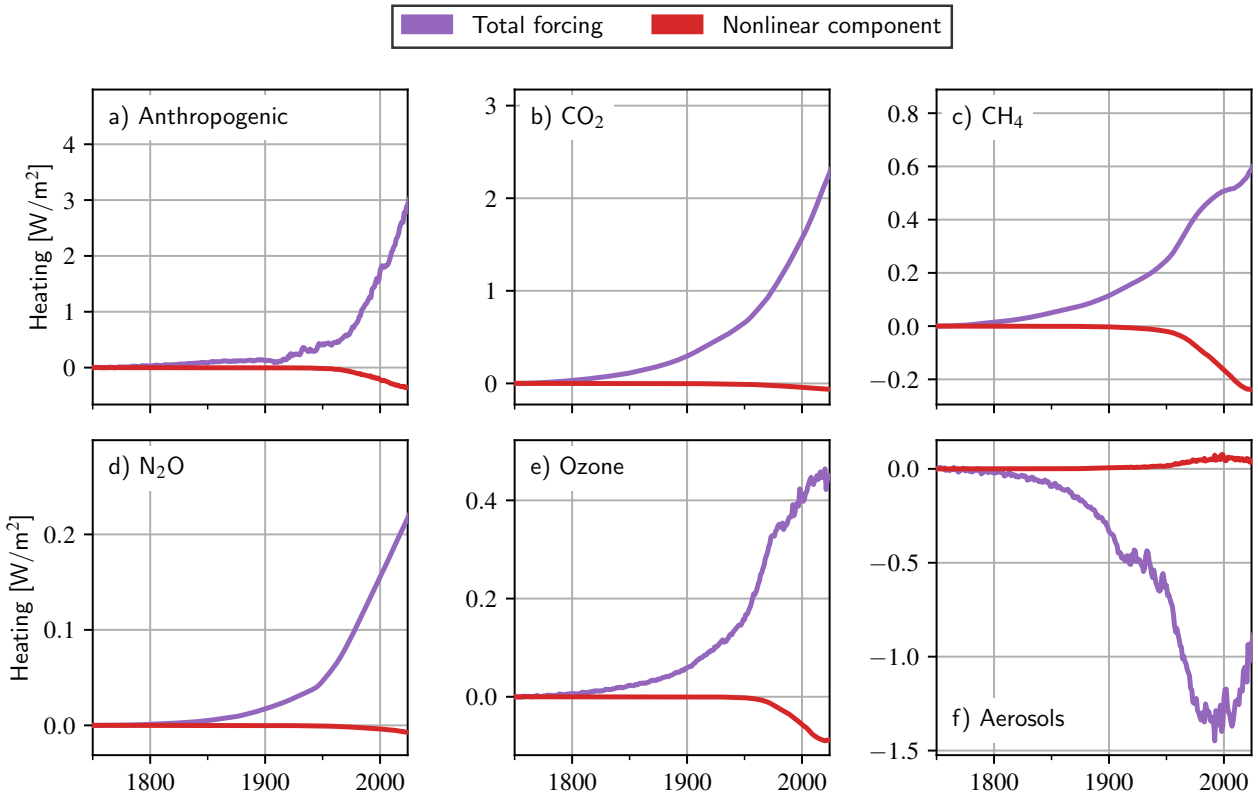

Fig. 11: Median estimates of the radiative heating (purple) due to all human activity (a) and the emissions of specific species (b-f) in the FaIR all activities experiment. The nonlinear component (red) arises from the interaction between fossil fuel emissions and emissions due to other activities. This nonlinearity makes the heating in the all-emissions experiment (purple) less than the sum of the heatings from the fossil-fuel and other-activities experiments. The nonlinear contribution (red) is calculated by subtracting the sum of the heatings from the fossil-fuel and other-activities experiments (not shown) from the forcing found when all emissions are considered together (purple). In the results presented in the main text, this nonlinear component has been removed in equal parts from the fossil-fuel and other-activities experiments (see Methods).

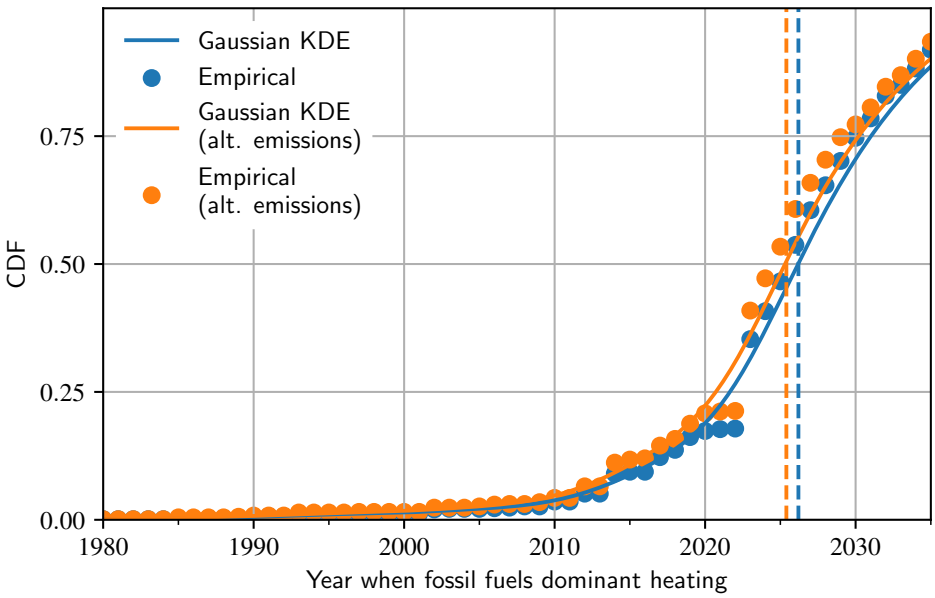

Fig. 12: Cumulative distribution function (CDF) of the projected year when the heating from fossil fuels equals the heating from other activities in the FaIR ensemble, analyzed under two different emissions decompositions: ambiguous emissions assigned to other activities (blue) and ambiguous emissions assigned to fossil fuels (orange); see Table 1 for details. Both the empirical CDF (circles) and a Gaussian kernel density estimate (KDE; solid curves), fitted with bandwidth determined by Silverman's rule, are shown. Differentiating this CDF yields the PDF in Figure 1. Dashed lines represent the median estimates for each decomposition. In both scenarios, it is likely (>50% chance) that fossil fuels will become the dominant source of heating within this decade.